Development and Validation of a Novel 3-Gene Prognostic Model for Pancreatic Adenocarcinoma Based on Ferroptosis-Related Genes

Jihua Yang
Fifth Affiliated Hospital of Sun Yat-sen University
Xiaohong Wei
Fifth Affiliated Hospital of Sun Yat-sen University
Fang Hu
Fifth Affiliated Hospital of Sun Yat-sen University
Dong Wei
Eastern Hepatobiliary Surgey Hospital, the Second Military Medical University https://orcid.org/0000-0001-6349-1423
Liao Sun (sunliao@mail.sysu.edu.cn)
The Fifth Affiliated Hospital of Sun Yat-sen University https://orcid.org/0000-0001-9458-020X

Primary research

Keywords: pancreatic adenocarcinoma, ferroptosis, prognosis, bioinformatics, genes.

Posted Date: October 21st, 2021

DOI: https://doi.org/10.21203/rs.3.rs-961571/v1

Version of Record: A version of this preprint was published at Cancer Cell International on January 15th, 2022. See the published version at https://doi.org/10.1186/s12935-021-02431-8.

Abstract

Background: Molecular markers play an important role in predicting clinical outcomes in pancreatic adenocarcinoma (PAAD) patients. Analysis of the ferroptosis-related genes may provide novel potential targets for the prognosis and treatment of PAAD.

Methods: RNA-sequence data of PAAD was downloaded from The Cancer Genome Atlas (TCGA) and Gene Expression Omnibus (GEO) public databases. The PAAD samples were clustered by a non-negative matrix factorization (NMF) algorithm. The R software package clusterProfiler was used for functional enrichment analysis. By LASSO regression, we established a multi-gene prognostic model, and the model was validated by qPCR and immunohistochemistry and T3M4 cell line.

Results: Three molecular subtypes were identified, and a 3-gene signature model (ALOX5, ALOX12, and CISD1) was constructed. The prognostic model showed good independent prognostic ability in PAAD. In the GSE62452 external validation set, the molecular model also showed good risk prediction. The predictive efficiency of the 3-gene signature-based nomogram was significantly better than that of traditional clinical features. Finally, qPCR and immunohistochemical staining and cell function results suggested that ALOX5 may be an oncogene and ALOX12 and CISD1 may be tumor suppressor genes.

Conclusions: We present a novel prognostic molecular model for PAAD based on ferroptosis-related genes, which serves as a potentially effective tool for prognostic differentiation in pancreatic cancer patients.

Background

Pancreatic cancer has a low 5-year survival rate and is one of the cancers that have high mortality [1]. In 2018, 458,918 new pancreatic cancer cases and 432,242 deaths due to it were reported globally [2]. Adenocarcinoma is the most common type of pancreatic cancer and accounts for >90% of the diagnosed pancreatic cancer cases. Although adjuvant chemotherapy and other multimodal treatments have been developed, surgery is still the most effective method for treating this disease [3]. Despite advances in the treatment of pancreatic adenocarcinoma (PAAD), the 5-year survival rate remains only 9% [4]. To tackle this, there is an urgent need to identify the prognostic biomarkers of PAAD. This would aid clinicians to predict the clinical outcomes promptly and accurately as well as initiate a protocol for a personalized treatment regimen.

Ferroptosis, a type of cell death, plays a vital role in inhibiting tumorigenesis by removing cells that either has a deficiency or overabundance of key nutrients or cells damaged by environmental pressure [5]. Unlike autophagy and apoptosis, ferroptosis is an iron (Fe) and reactive oxygen species (ROS)-dependent form of cell death, [6]. It regulates cell death through the overproduction of phospholipid hydroperoxides in a mechanism different from that of autophagy and apoptosis. It is induced in abnormal cells due to loss of the selective permeability of the plasma membrane and oxidative stress caused by intense

membrane lipid peroxidation [7]. Ferroptosis plays an important regulatory role in the occurrence and progression of tumors and provides a promising therapeutic strategy for PAAD [8, 9].

Many genes may contribute to the development of PAAD. Recent studies have shown that CA9, CXCL9, and GIMAP7 genes specifically regulate the expression of FoxO1, thereby regulating immune infiltration in PAAD [10]. Further, LINC01232 exerts oncogenic activity in PAAD by up-regulating the expression of TM9SF2 through the recruitment of eIF4A3 [11]. Moreover, over-expression of CBX3 induces in vitro proliferation, unanchored growth, migration, and invasion of PAAD cells, and in vivo growth of in situ PAAD tumors in mice [12].

With the development of next-generation sequencing technology, gene transcription profiles in PAAD can be better understood. Based on The Cancer Genome Atlas (TCGA) and the comprehensive Gene Expression Omnibus (GEO) databases, we identified ferroptosis-associated genes and constructed molecular subtypes of PAAD based on them. Finally, we established a 3-gene signature prognostic model and verified its ability to predict the prognostic risk of PAAD. This serves as a potentially effective tool for prognostic risk prediction in patients with pancreatic cancer.

Methods

Data source and processing

Expression data and corresponding clinical follow-up information from the TCGA-PAAD data set were downloaded using the UCSC genome browser database. GSE62452 chip data sets with survival time were selected from Gene Expression Omnibus (GEO) database. Henceforth, samples that lacked clinical follow-up information were removed and the expression of multiple gene symbols was considered the median value.

Molecular subtype identification using the non-negative matrix factorization algorithm

Firstly, 60 ferroptosis-related genes were retrieved from the literature [13, 14, 15, 16] (Table 1). Next, 58 ferroptosis-related genes with gene expression data were matched with the TCGA-PAAD data set, and PAAD samples were clustered by non-negative matrix factorization (NMF). The standard "Lee" was selected in the NMF method, and ten iterations were performed. The cluster number ‘k’ was set at 2-10, the average contour width of the common member matrix was determined by the R package "NMF", and the samples were divided into three categories.

Identification and functional analysis of differentially expressed genes (DEGs)

The limma package was used to analyze the differentially expressed genes (DEGs) in cluster 1, cluster 2, and cluster 3 among the molecular subtypes, based on the threshold false discovery rate (FDR) < 0.05 and | log2FC | > 0.5 filters. The DEGs shared by the three clusters were identified, and the Kyoto Encyclopedia of Genes and Genomes (KEGG) pathway analysis and gene ontology (GO) functional enrichment analysis were performed on them through the R package clusterProfiler (v3.16.1).

Comparative analysis of immune scores among molecular subtypes

The single-sample gene set enrichment analysis (ssGSEA) method of the GSVA (Gene Set Variation Analysis) package was used to identify the immune score-based relationships among the molecular subtypes in the TCGA-PAAD data set. The scores of 28 immune cells were assessed [17] and then the differences in immune scores among the molecular subtypes were compared.

Training set and internal test set construction

A total of 173 samples in the TCGA-PAAD data set were divided into a training set and a test set. To prevent the random allocation bias from affecting the stability of subsequent modeling, all samples were put back into random grouping, two hundred times in advance. Using the training data set, a univariate Cox proportional risk regression model was constructed for ferroptosis-related genes (n=60) and survival data was constructed using the coxph function with survival R package. Since 58 ferroptosis-related genes had expression profile data in our data set, only these were selected for the univariate Cox regression analysis, and $P < 0.05$ was selected as the threshold for filtering. The R software package “glmnet” was used to carry out the LASSO Cox regression analysis. We first analyzed the changing trajectory of each independent variable, and later used the 5-fold cross-validation to build a model and analyze the confidence interval under each lambda. The target genes were selected by multivariate Cox regression analysis, and a prognostic Kaplan-Meier (KM) curve was established.

3-gene signature robustness in different data sets

The risk scores of each sample were calculated separately based on the expression level of the sample. KM-curve analysis showed significant differences between the high and low expression groups. Furthermore, we used the R software package timeROC to conduct ROC analysis of the prognostic classification of the risk score and analyze the prognostic classification efficiency at 1-year, 3-years, and 5-years. The model and the survival coefficient, developed using the training dataset, were adopted to evaluate the entire TCGA-PAAD data set, calculate the risk score of each sample and establish the risk score distribution of the samples. The independent GSE62452 data set was used to analyze the robustness of the model.

Univariate and multivariate analyses of the 3-gene signature

To identify the independence of the 3-gene signature model in clinical applications, we performed Cox regression analysis on the TCGA-PAAD training dataset. Based on the results of univariate and multivariate analyses, we used the TCGA-PAAD training dataset to construct a histogram. In addition, corrected curves were used to analyze the prediction accuracy of nomogram at 1, 3, and 5 years.

Tissue samples

PAAD tissues were derived from surgically resected specimens and snap-frozen in liquid nitrogen until RNA extraction. None of the patients received chemotherapy or radiation therapy before surgery. All

patients signed informed consent forms provided by the Eastern Hepatobiliary Surgery Hospital. This study was approved by the Ethics Committee of the Eastern Hepatobiliary Surgery Hospital.

RNA isolation and RT-qPCR analysis

RNA was extracted from tissues using the TRIzol reagent (Invitrogen, Carlsbad, CA, USA) and was reverse-transcribed into cDNA using the QuantiTect Reverse Transcription Kit (Qiagen, Valencia, CA, USA). Quantitative PCR (qPCR) uses real-time fluorescence to measure the quantity of DNA present at each cycle during a PCR. Real-time qPCR analyses were quantified with SYBR-Green (Takara, Otsu, Shiga, Japan), and expression levels were normalized to GAPDH levels.

Immunohistochemistry

Pancreatic cancer samples were fixed in 10% formalin, embedded in paraffin, and processed into 5-μm sequential sections. The samples were de-waxed with ethanol and blocked to inhibit the endogenous peroxidase activity. After this, samples were heated in a microwave for antigen retrieval, cooled to room temperature, and blocked using goat serum for 30 min at 37°C. The samples were incubated overnight at 4°C with rabbit anti-ALOX5 (ab169755), anti-ALOX12 (ab211506), and anti-CISD1 (ab203096) (Abcam, USA) (1:200), followed by incubation with horseradish peroxidase-coupled goat anti-rabbit secondary antibody at 37°C for 30 min. The samples were then stained with 3,3’-Diaminobenzidine (DAB). Cell nuclei were stained blue with hematoxylin. The sections were then dehydrated, cleared with xylene, and mounted. ALOX5, ALOX12, and CISD1 expressions were determined by immunohistochemistry (IHC) using the streptavidin peroxidase method, with adjacent tissues serving as the controls. The experimental procedure was performed as per the manufacturer’s instructions. Image-Pro Plus 6.0 Software (Media Cybernetics, USA) was used to analyze protein expression and perform statistical analysis of the results obtained by IHC.

Cell culture and Transfection

Te human PAAD cell line T3M4 was provided by the National Collection Authenticated Cell Cultures (Shanghai, China). The cell lines were cultured in DMEM (dulbecco's modified eagle medium) (Gibco, Grand Island, NY, USA). supplemented with 10% fetal bovine serum (Invitrogen, San Diego, CA) at 37 °C under 5% CO2 in a humidified incubator. Si-CISD1 (No: CAT#: SR310990), Si-ALOX5 (No: CAT#: SR319325) and Si-ALOX12 (No: CAT#: SR300166) were purchased from Origene (Beijing, China). Transfection was performed using Lipofectamine 3000 reagent (No. L3000015, Invitrogen, China) according to the instructions.

Cell viability assays

Cells were seeded into 96-well plates at a concentration of 2000 cells per well. Cell viability was detected by Cell Counting Kit-8 assay (CCK-8, Dojindo, Japan) according to the manufacturer’s protocol. Te absorbance at 450 nm was measured using an automatic microplate reader (BioTek, Winooski, VT, USA).

Cell migration and invasion assays

For the migration assay, 800 μl DMEM with 20% serum was added to the lower chamber of a Transwell plate (Corning, NY, USA), and T3M4 cells were added in the upper chamber. After incubation for 24 h at 37 °C, the Transwell chamber was removed, and the relative cell density was measured by ImageJ (National Institute of Health, USA). ImageJ software was used to analyze and calculate the migration and invasion area of the transwell cultured with T3M4 cells. The migration and invasion index (%) depicts a proportion of an area where cells have invaded in percentage and is calculated as epithelium area divided by the total area of invaded cells area. The area describes the overall area (μm^2) of invaded cells. Evaluation of invasive capacity was performed by counting invading cells under a microscope (40 × 10). Five random fields of view were analyzed for each chamber.

Statistical analysis

All data were analyzed using the SPSS 21.0 statistical software program (IBM Corporation, Armonk, NY, USA). Graphs were generated with GraphPad Prism 8.0 software (GraphPad Software, Inc., San Diego, CA). Student's t-tests were performed. For a two-tailed t-test, $p<0.05$ was essential for considering the results to be statistically significant.

Results

Sample information statistics

After data preprocessing, there were 173 samples in TCGA-PAAD, with 88 samples in the training set and 85 samples in the test set. GSE62452 included 66 samples. The clinical statistical information of the samples is shown in Table 1.

Identification of three molecular subtypes

The 173 samples were divided into 3 categories: C1, C2, and C3. The expression of prognostic ferroptosis-related genes in the three categories is shown in Fig 1A. The figure shows that the expression levels of these genes are different in the 3 subtypes and that most of the genes are highly expressed in the C1 subgroup. Further analysis of the prognostic relationships between the two groups showed significant differences in C1, C2, and C3 (Fig 1B, log-rank test, $P < 0.05$). A clustering heat map of the 58 iron ferroptosis-related genes is shown in Fig 1 C.

Analysis of DEGs among subtypes

With the help of the limma package, 4,903 DEGs were identified between Cluster 1 and Cluster 2, among which 2,717 genes were up-regulated and 2,186 genes were down-regulated (Fig 2 A, D). There were 6,572 DEGs between Cluster 1 and Cluster 3, among which 4,963 genes were up-regulated and 1,609 genes were down-regulated (Fig 2 B, E). Between Cluster 2 and Cluster 3 there were 3,473 DEGs, among which

2,633 genes were up-regulated and 840 genes were down-regulated (Fig 2 C, F). After taking the intersection of all three clusters 230 genes were obtained.

KEGG pathway analysis and GO functional enrichment analysis were performed on the 230 DEGs in the PAAD subtype group. A total of 179 GO-BP pathways, 47 GO-CC pathways, and 67 GO-MF pathways were annotated (Figure 3 A). 14 KEGG pathways were identified, 6 of which were significant (FDR<0.05) (Figure 3 B). The detailed information is shown in Table 2.

Comparative analysis of immune scores among molecular subtypes

Immune scores in the TCGA-PAAD dataset were identified. The GSVA score of 28 immune cells was used to compare the differences among the molecular subtypes. The immune score of the C1 subtype was lower than that of the C2 (Fig 4A) and C3 subtype (Fig 4B). The immune score of the C2 subtype was lower than that of the C3 subtype (Fig 4C). Additionally, we constructed a heat map of the immune score results for the three subtypes (Fig 4D-F).

Construction of a 3-gene signature

Ultimately, 10 genes were identified to be associated with prognosis. Next, LASSO regression was used to further compress the 10 genes to reduce the number of genes in the risk model. The changing trajectory of each independent variable is shown in Fig 5A, which indicates that with a gradual increase in lambda, the number of independent variable coefficients approaching zero gradually increases. We used 5-fold cross-validation to construct a model and analyze the confidence interval under each lambda (Fig 5B). The figure indicates that the model reached the optimal value at lambda= -3.75. Hence, we selected 5 genes at lambda= -3.75 as target genes and further selected 3 genes (ALOX5, ALOX12, and CISD1) by multivariate Cox regression analysis. Prognostic KM-curves of the three genes are shown in Fig 5C-E, and all three genes could significantly improve the performance of distinguishing between the low-risk groups (LRG) and high-risk groups (HRG) in the training sample ($P < 0.05$). The final model based on the 3-gene signature was as follows:

RiskScore=0.289* ALOX5+-1.359*ALOX12+(-1.053)* CISD1

Further, we calculated the risk score of each sample based on the expression level of the sample. The risk score distribution of the training set is shown in Fig 6B. The figure indicates that the risk of death for a patient with a high-risk score was significantly higher than that of a patient with a low-risk score. This suggests that a sample with a high-risk score shows a worse prognosis. KM-curve analysis showed that there were significant differences between the high and low-risk groups (Fig 6A, P =0.006). (Fig 6C). The model had a very high AUC (AUC for 1 year=0.547, AUC for 3 years=0.815, AUC for 5 years=0.976) The risk score distribution of the entire TCGA-PAAD dataset is shown in Fig 6E, which also indicates that samples with a high-risk score had a worse prognosis. KM-curve analysis showed that there were significant differences between the high and low-risk groups (Fig 6D, P <0.001). The classification efficiencies at 1-year, 3-years, and 5-years were 0.741, 0.788, and 0.774 (Fig 6F), respectively.

Analysis of the GSE62452 showed that the risk score distribution was consistent with that of the training set and that the high-risk score samples had a worse prognosis (Fig 6H). KM-curve analysis showed that there were significant differences between the high and low-risk groups (Fig 6G, P =0.016). Analysis of the 1-year, 3-years, and 5-years prognostic prediction classification efficiencies (Fig 6I) indicated that the model had relatively high AUC at 3 years and 5 years (0.718 and 0.743, respectively).

Risk model analysis and model comparison

Based on the 3-gene signature model, samples could be divided into low- and high-risk groups according to age, sex, grade, N stage, T stage, or clinical stage (Figure 7A-L, P < 0.05). This further indicated that our model had good predictive power in different clinical subgroups. The risk score had a significant correlation with age, sex, grade, T stage, and clinical-stage but no significant correlation was with the N stage (Figure 8 A-F, P <0.05). Both, univariate and multivariate Cox regression analyses, indicated that our model based on the 3-gene signature is an independent risk factor for prognosis in pancreatic cancer patients (Fig 9A-B). Further, the TCGA-PAAD training set was used to construct a nomogram (Fig 9C), which indicated that the risk model based on the 3 genes can accurately predict the prognosis of pancreatic cancer. In addition, we used corrected curves to analyze the prediction accuracy of the nomogram at 1, 3, and 5 years. The results indicated that the histogram had good prediction performance (Fig 9D). Moreover, the results of decision curve analysis (DCA) at 1-year, 3-years, and 5-years (Fig 9E) also indicated that the prediction efficiency of the histogram was good.

For comparison with our model, we selected two prognostic risk models: 20 gene signatures [PMID 25587357] and 36 gene signatures [PMID32310997]. Survival analysis indicated that the PAAD prognosis of the high-risk score and low-risk score groups was different except for the 36-gene signature and 20-gene signature models (log-rank p <0.05). For the 36-gene signature model, the 1-, 3-, and 5-year AUC values were lower than our model. Moreover, the 1- and 3-year AUC values in the 20-gene signature were lower than our model. This proves that our model, with a reasonable number of genes, yields a more effective result (Figure 10).

The expression and biological function of signature genes in PAAD

To verify that ALOX5 expression is upregulated and investigate whether ALOX12 and CISD1 are downregulated in pancreatic cancer tissue, 10 pancreatic cancer tissue specimens were tested. The results obtained with qPCR (Fig 11A-C) and IHC (Fig 11D-F) assays showed that ALOX5 was highly expressed regardless of whether ALOX12 and CISD1 were expressed at low levels in these pancreatic cancer tissue samples. Clinical details of these 10 patients are contained in the Additional file. To clarify the functional role of signature genes in PAAD cells, we used Cancer Cell Line Encyclopedia (CCLE) database to analyze the expression of ALOX5, ALOX12 and CISD1 in pancreatic cancer cells, and found that the expression of ALOX5, ALOX12 and CISD1 was relatively highly expressed in T3M4 cells (Figure 12). siRNA was used to reduce the expression of ALOX5, ALOX12 and CISD1 in T3M4 cells. CCK8 and transwell assays were used to determine the proliferation, invasion and migration ability of T3M4 cells. The results showed that reduced ALOX5 (Fig 13A, D and G) expression significantly inhibited the

proliferation, invasion and migration ability of T3M4 cells ,and reduced ALOX12 (Fig 7B,E and H) and CISD1 (Fig 13C,F and I) expression significantly increased proliferation, invasion and migration ability of T3M4 cells.

Discussion

Ferroptosis is an iron oxide-dependent form of regulated cell death (RCD). It is the link that connects metabolism, redox biology, and human health. Accumulating evidence indicates that ferroptosis can be triggered to treat cancer to eradicate aggressive malignancies that are resistant to conventional therapies [25]. It is characterized by the accumulation of ROS and lipid peroxidation products to lethal levels. Although ferroptosis plays an important role in maintaining the survival of normal cells and tissues, it has been increasingly recognized that some carcinogenic pathways are related to ferroptosis, making cancer cells vulnerable to ferroptosis death [26, 27]. In pancreatic cancer, the process of iron death significantly promotes disease progression and may be a potential strategy for inhibiting pancreatic cancer development. For example, GOT1 inhibition promotes pancreatic cancer cell death by ferroptosis. In this study, we identified a ferroptosis related gene signature for predicting the prognosis of pancreatic adenocarcinoma patients.

Due to the insidious and aggressive nature of PAAD, it is difficult to detect and prevent PAAD at an early stage. At the time of consultation, approximately 80% of patients have locally advanced or metastatic cancer [18]. Although multimodal therapy has been improved, surgery remains an effective therapeutic strategy for this disease. Even in conjunction with adjuvant therapy, pancreatic surgery can improve five-year survival by only 20% [19]. Therefore, prognostic signatures for PAAD patients are urgently needed. With the advancement in the field of bioinformatics and sequencing technology, several potential prognostic evaluation methods for PAAD patients have been developed [20, 21, 22]. However, mostly genome or transcriptome parameters are analyzed in these methods, with no consideration of biological processes. Therefore, these models do not analyze the characteristics features of PAAD. Ferroptosis is a significant biological hallmark of tumors and has been demonstrated to be of value in evaluating the prognosis of patients with PAAD [23, 24]. In this study, ferroptosis-related genes were collected, and gene expression data from public databases such as the TCGA and GEO were used to construct PAAD molecular subtypes based on ferroptosis-related genes. Next, LASSO regression was used to further compress the 10 genes to reduce the number of genes in the risk model. We used 5-fold cross-validation to construct a model and analyze the confidence interval under each lambda. The indicates that the model reached the optimal value at lambda= -3.75. Hence, we selected 5 genes at lambda= -3.75 as target genes and further selected 3 genes (ALOX5, ALOX12, and CISD1) by multivariate Cox regression analysis, and all three genes could significantly improve the performance of distinguishing between the LRG and HRG in the training sample ($P < 0.05$). The final model based on the 3-gene signature was as follows: RiskScore=0.289* ALOX5+(-1.359)*ALOX12+(-1.053)* CISD1 We found that the constructed 3-gene signature model achieved an accurate prognostic assessment of PAAD samples relative to the other methods. We also compared with previously developed gene-based signatures for PAAD, with two prognostic risk models: 20 and 36 gene signature which result showed our model obtained a more

effective result with the reasonable number of genes. The performance of our prognostic risk model was further verified by using validation set data and qPCR and IHC experiments, also with pancreatic cancer cell lines *vitro* validation. The functional study shown that expression of ALOX5, ALOX12, and CISD1 can regulate the migration and invasion ability of PAAD cells. Our signature is more accurate than other, and we established a more reasonable and efficient model with fewer genes. Our 3-gene signature model, with fewer genes, is more accurate, reasonable, and efficient as compared to other established models.

The signature we constructed contained three genes, namely, ALOX5, ALOX12, and CISD1, all of which are closely related to tumors genesis and development. 5-Lipoxygenase (ALOX5) is a non-heme iron-containing dioxygenase that catalyzes the peroxidation of polyunsaturated fatty acids, such as arachidonic acid [28]. ALOX5 is a key enzyme that mediates lipid peroxidation and thereby leads to cell death. [29]. Available evidence shows that lipid peroxidation evokes multiple types of cell death including apoptosis, pyroptosis, and ferroptosis [30]. It has also been reported that high ALOX5 expression is significantly associated with a poor prognosis in colorectal cancer, gastric cancer, clear cell renal cell carcinoma, papillary thyroid carcinoma, and other tumors [31, 32, 33, 34]. ALOX12 gene encodes the enzyme arachidonate 12-lipoxygenase. This enzyme acts on various polyunsaturated fatty acid substrates to produce biologically active lipid intermediates, including eicosanoids and lipoxins. The ALOX12 protein plays an important role in inflammation and oxidation. Abnormal DNA methylation and genetic variation in ALOX12 are associated with various human diseases and pathological phenotypes, such as cardiovascular disease, diabetes, neurodegenerative disease, respiratory disease, cancer, and infection [35]. Many studies indicate the abnormal expression of ALOX12 in tumors, suggesting that ALOX12 may be a potential marker for many varieties of cancers. Studies in xenotransplantation models show that ALOX12 inactivation reduces the p53-mediated ferroptosis induced by ROS stress, and thus eliminates the p53-dependent tumor growth inhibition [36]. Compared with pancreatic cancer precursors and normal pancreatic ducts, the expression of ALOX12 in pancreatic cancers is significantly down-regulated and inhibits the proliferation of PAAD cells [37]. CISD1 (mitoNEET) belongs to a newly discovered class of iron-thionine (2Fe-2S). It is essential for regulating iron and ROS homeostasis in cells and plays a key role in promoting cancer cell proliferation and supporting tumor growth and metastasis [38]. Additionally, CISD1 is overexpressed in both lung adenocarcinoma and breast cancer [39, 40].

In this study, we present evidence that ALOX5, ALOX12, and CISD1 may have prognostic value in PAAD. Specifically, our in vitro results suggest that ALOX5 may be an oncogene, while ALOX12 and CISD1 may be tumor suppressor genes in PAAD. The results of our study indicate that the established 3-gene signature model could be an effective prognostic tool for patients with PAAD. However, the limitations associated with this study emphasize the need for additional analysis before the clinical application of this signature. The samples used in our study were obtained retrospectively and the study solely focused on the prognostic value and clinical significance of ferroptosis. To validate our findings for clinical applications, we need to include prospective samples and evaluate the prognostic values of other biological processes characteristic to the development of cancer.

Conclusion

In conclusion, we propose a 3-gene signature (ALOX5, ALOX12, and CISD1) predictive model based on ferroptosis-related genes in PAAD. Despite the many drawbacks of the current analysis, this model may serve as an interesting molecular diagnostic tool to assess the prognosis and possible risk factors of PAAD.

Abbreviations

PAAD
pancreatic adenocarcinoma
TCGA
The Cancer Genome Atlas
GEO
Gene Expression Omnibus
NMF
Non-negative matrix factorization
ROS
Reactive oxygen species
DEGs
Differentially expressed genes
FDR
False discovery rate
KEGG
Kyoto Encyclopedia of Genes and Genomes
GO
Gene ontology
ssGSEA
single-sample gene set enrichment analysis
GSVA
Gene Set Variation Analysis
KM
Kaplan-Meier
IHC
Immunohistochemistry
CCK-8
Cell Counting Kit-8
LRG
Low-risk groups
HRG

High-risk groups

DCA

Decision curve analysis

CCLE

Cancer Cell Line Encyclopedia

RCD

Regulated cell death

Declarations

Ethics approval and consent to participate

The research protocol was approved by the Ethics Committee of Shanghai Eastern Hepatobiliary Surgery Hospital. All the patients provided written informed consent. The study was conducted according to the guidelines of the Declaration of Helsinki and approved by the Institutional Review Board.

Consent for publication

All authors consented to the publication of the paper.

Availability of data and materials

The results shown here are in whole or part based upon data generated by TCGA (https://www.cancer.gov/tcga), KEGG (https://www.genome.jp/kegg), GO (http://geneontology.org), GEO (https://www.ncbi.nlm.nih.gov/geo).

Competing interests

The authors declare that the research was conducted in the absence of any commercial or financial relationships that could be construed as a potential conflict of interest.

Funding

This work was supported by the Guangdong Province National Natural Science Foundation of China (Grant 2018A0303130263).

Author's contributions

Conceptualization, J.Y., X.W., F.H., W.D., and L.S.; data curation, J.Y. and X.W; formal analysis, J.Y. and X.W.; investigation, J.Y. and X.W.; methodology, J.Y. and X.W.; project administration, J.Y., X.W., F.H. and W.D.; resources, W.D., and L.S.; software, J.Y. and F.H.; supervision, W.D. and L.S.; validation, J.Y., X.W. and L.S.; writing—original draft, J.Y.; writing—review and editing, W.D. and L.S. All authors have read and agreed to the published version of the manuscript.

Acknowledgments

We thank the Ethics Committee of Shanghai Eastern Hepatobiliary Surgery Hospital to provide pathological tissues. We thank the members LeiLei Liang and Meng Wang of the National Cancer Center lab for scientific discussion with sincerely help.

References

1.Wei K, Hackert T. Surgical Treatment of Pancreatic Ductal Adenocarcinoma. Cancers (Basel). 2021 Apr 20;13(8):1971. doi: 10.3390/cancers13081971. PMID: 33923884; PMCID: PMC8074119.

2.Bray F, Ferlay J, Soerjomataram I, Siegel RL, Torre LA, Jemal A. Global cancer statistics 2018: GLOBOCAN estimates of incidence and mortality worldwide for 36 cancers in 185 countries. CA Cancer J Clin. 2018;68:394–424.

3.Vincent A., Herman J., Schulick R., Hruban R., Goggins M. Pancreatic cancer. Lancet. 2011;378:607–620. doi: 10.1016/S0140-6736(10)62307-0.

4.Rawla P, Sunkara T, Gaduputi V. Epidemiology of Pancreatic Cancer: Global Trends, Etiology and Risk Factors. World J Oncol. 2019;10:10–27.

5.Fearnhead HO, Vandenabeele P, Vanden TB. How do we fit ferroptosis in the family of regulated cell death? Cell Death Differ. 2017;24:1991–1998. doi: 10.1038/cdd.2017.149.

6.Yu H, Guo P, Xie X, Wang Y, Chen G. Ferroptosis, a new form of cell death, and its relationships with tumourous diseases. J Cell Mol Med. 2017;21:648–657. doi: 10.1111/jcmm.13008.

7.Yang WS, Stockwell BR. Synthetic lethal screening identifies compounds activating iron-dependent, nonapoptotic cell death in oncogenic-RAS-harboring cancer cells. Chem Biol. 2008;15:234–245. doi: 10.1016/j.chembiol.2008.02.010.

8.Li J, Cao F, Yin HL, Huang ZJ, Lin ZT, Mao N, Sun B, Wang G. Ferroptosis: past, present and future. Cell Death Dis. 2020 Feb 3;11(2):88. doi: 10.1038/s41419-020-2298-2. PMID: 32015325; PMCID: PMC6997353.

9.Yamaguchi Y, Kasukabe T, Kumakura S. Piperlongumine rapidly induces the death of human pancreatic cancer cells mainly through the induction of ferroptosis. Int J. Oncol. 2018;52:1011–1022.

10.Meng Z, Ren D, Zhang K, Zhao J, Jin X, Wu H. Using ESTIMATE algorithm to establish an 8-mRNA signature prognosis prediction system and identify immunocyte infiltration-related genes in Pancreatic adenocarcinoma. Aging (Albany NY). 2020 Mar 17;12(6):5048-5070. doi: 10.18632/aging.102931. Epub 2020 Mar 17. PMID: 32181755; PMCID: PMC7138590.

11.Li Q, Lei C, Lu C, Wang J, Gao M, Gao W. LINC01232 exerts oncogenic activities in pancreatic adenocarcinoma via regulation of TM9SF2. Cell Death Dis. 2019 Sep 20;10(10):698. doi: 10.1038/s41419-019-1896-3. PMID: 31541081; PMCID: PMC6754375.

12.Chen LY, Cheng CS, Qu C, Wang P, Chen H, Meng ZQ, Chen Z. Overexpression of CBX3 in Pancreatic Adenocarcinoma Promotes Cell Cycle Transition-Associated Tumor Progression. Int J Mol Sci. 2018 Jun 14;19(6):1768. doi: 10.3390/ijms19061768. PMID: 29903985; PMCID: PMC6032220.

13.Stockwell BR, Friedmann Angeli JP, Bayir H, Bush AI, Conrad M, Dixon SJ. et al. Ferroptosis: A Regulated Cell Death Nexus Linking Metabolism, Redox Biology, and Disease. Cell. 2017;171:273–85. [PMC free article] [PubMed] [Google Scholar]

14.Hassannia B, Vandenabeele P, Vanden Berghe T. Targeting Ferroptosis to Iron Out Cancer. Cancer Cell. 2019;35:830–49. [PubMed] [Google Scholar]

15.Bersuker K, Hendricks JM, Li Z, Magtanong L, Ford B, Tang PH. et al. The CoQ oxidoreductase FSP1 acts parallel to GPX4 to inhibit ferroptosis. Nature. 2019;575:688–92. [PMC free article] [PubMed] [Google Scholar]

16.Doll S, Freitas FP, Shah R, Aldrovandi M, da Silva MC, Ingold I. et al. FSP1 is a glutathione-independent ferroptosis suppressor. Nature. 2019;575:693–8. [PubMed] [Google Scholar]

17.Charoentong P, Finotello F, Angelova M, Mayer C, Efremova M, Rieder D, Hackl H, Trajanoski Z. Pan-cancer Immunogenomic Analyses Reveal Genotype-Immunophenotype Relationships and Predictors of Response to Checkpoint Blockade. Cell Rep. 2017 Jan 3;18(1):248-262. doi: 10.1016/j.celrep.2016.12.019. PMID: 28052254.

18.Fong ZV, Ferrone CR. Surgery After Response to Chemotherapy for Locally Advanced Pancreatic Ductal Adenocarcinoma: A Guide for Management. J Natl Compr Canc Netw. 2021 Apr 1;19(4):459-467. doi: 10.6004/jnccn.2021.7009. PMID: 33845457.

19.De Dosso S., Siebenhuner A.R., Winder T., Meisel A., Fritsch R., Astaras C., Szturz P., Borner M. Treatment landscape of metastatic pancreatic cancer. Cancer Treat Rev. 2021;96:102180. doi: 10.1016/j.ctrv.2021.102180.

20.Wu M, Li X, Zhang T, Liu Z, Zhao Y. Identification of a Nine-Gene Signature and Establishment of a Prognostic Nomogram Predicting Overall Survival of Pancreatic Cancer. Front Oncol. 2019 Sep 27;9:996. doi: 10.3389/fonc.2019.00996. PMID: 31612115; PMCID: PMC6776930.

21.Lv S, Zhang G, Xie L, Yan Z, Wang Q, Li Y, Zhang L, Han Y, Li H, Du Y, Yang Y, Guo X. High TXLNA Expression Predicts Favourable Outcome for Pancreatic Adenocarcinoma Patients. Biomed Res Int. 2020 Feb 25;2020:2585862. doi: 10.1155/2020/2585862. PMID: 32185195; PMCID: PMC7060861.

22.Wang ZX, Deng TX, Ma Z. Identification of a 4-miRNA signature as a potential prognostic biomarker for pancreatic adenocarcinoma. J Cell Biochem. 2019 Oct;120(10):16416-16426. doi: 10.1002/jcb.28601. Epub 2019 Jul 11. PMID: 31297864.

23.Song Z, Xiang X, Li J, Deng J, Fang Z, Zhang L, Xiong J. Ruscogenin induces ferroptosis in pancreatic cancer cells. Oncol Rep. 2020 Feb;43(2):516-524. doi: 10.3892/or.2019.7425. Epub 2019 Dec 10. PMID: 31894321; PMCID: PMC6967081.

24.Ye Z, Zhuo Q, Hu Q, Xu X, Mengqi Liu, Zhang Z, Xu W, Liu W, Fan G, Qin Y, Yu X, Ji S. FBW7-NRA41-SCD1 axis synchronously regulates apoptosis and ferroptosis in pancreatic cancer cells. Redox Biology. 2021 Jan;38:101807. doi: 10.1016/j.redox.2020.101807. Epub 2020 Nov 24. PMID: 33271455; PMCID: PMC7710650.

25.Liang C, Zhang X, Yang M, Dong X. Recent Progress in Ferroptosis Inducers for Cancer Therapy. Adv Mater. 2019 Dec;31(51):e1904197. doi: 10.1002/adma.201904197. Epub 2019 Oct 8. PMID: 31595562.

26.Stockwell BR, Friedmann Angeli JP, Bayir H, Bush AI, Conrad M, Dixon SJ, Fulda S, Gascón S, Hatzios SK, Kagan VE, Noel K, Jiang X, Linkermann A, Murphy ME, Overholtzer M, Oyagi A, Pagnussat GC, Park J, Ran Q, Rosenfeld CS, Salnikow K, Tang D, Torti FM, Torti SV, Toyokuni S, Woerpel KA, Zhang DD. Ferroptosis: A Regulated Cell Death Nexus Linking Metabolism, Redox Biology, and Disease. Cell. 2017 Oct 5;171(2):273-285. doi: 10.1016/j.cell.2017.09.021. PMID: 28985560; PMCID: PMC5685180.

27.Dixon SJ, Lemberg KM, Lamprecht MR, Skouta R, Zaitsev EM, Gleason CE, Patel DN, Bauer AJ, Cantley AM, Yang WS, Morrison B 3rd, Stockwell BR. Ferroptosis: an iron-dependent form of nonapoptotic cell death. Cell. 2012 May 25;149(5):1060-72. doi: 10.1016/j.cell.2012.03.042. PMID: 22632970; PMCID: PMC3367386.

28.Sun QY, Zhou HH, Mao XY. Emerging Roles of 5-Lipoxygenase Phosphorylation in Inflammation and Cell Death. Oxid Med Cell Longev. 2019 Nov 29;2019:2749173. doi: 10.1155/2019/2749173. PMID: 31871543; PMCID: PMC6906800.

29.Gaschler M. M., Stockwell B. R. Lipid peroxidation in cell death. Biochemical and Biophysical Research Communications. 2017;482(3):419–425. doi: 10.1016/j.bbrc.2016.10.086.

30.Mao X. Y., Zhou H. H., Jin W. L. Redox-related neuronal death and crosstalk as drug targets: focus on epilepsy. Frontiers in Neuroscience. 2019;13:p. 512. doi: 10.3389/fnins.2019.00512.

31.Wang D, Li Y, Zhang C, Li X, Yu J. MiR-216a-3p inhibits colorectal cancer cell proliferation through direct targeting COX-2 and ALOX5. J Cell Biochem. 2018 Feb;119(2):1755-1766. doi: 10.1002/jcb.26336. Epub 2017 Sep 11. PMID: 28786533.

32.Merchant N, Bhaskar LVKS, Momin S, Sujatha P, Reddy ABM, Nagaraju GP. 5-Lipoxygenase: Its involvement in gastrointestinal malignancies. Crit Rev Oncol Hematol. 2018 Jul;127:50-55. doi:

10.1016/j.critrevonc.2018.05.012. Epub 2018 May 18. PMID: 29891111.

33.Cui H, Shan H, Miao MZ, Jiang Z, Meng Y, Chen R, Zhang L, Liu Y. Identification of the key genes and pathways involved in the tumorigenesis and prognosis of kidney renal clear cell carcinoma. Sci Rep. 2020 Mar 6;10(1):4271. doi: 10.1038/s41598-020-61162-4. PMID: 32144299; PMCID: PMC7060270.

34.Reyes I, Reyes N, Suriano R, Iacob C, Suslina N, Policastro A, Moscatello A, Schantz S, Tiwari RK, Geliebter J. Gene expression profiling identifies potential molecular markers of papillary thyroid carcinoma. Cancer Biomark. 2019;24(1):71-83. doi: 10.3233/CBM-181758. PMID: 30614796.

35.Zheng Z, Li Y, Jin G, Huang T, Zou M, Duan S. The biological role of arachidonic acid 12-lipoxygenase (ALOX12) in various human diseases. Biomed Pharmacother. 2020 Sep;129:110354. doi: 10.1016/j.biopha.2020.110354. Epub 2020 Jun 12. PMID: 32540644.

36.Chu B, Kon N, Chen D, Li T, Liu T, Jiang L, Song S, Tavana O, Gu W. ALOX12 is required for p53-mediated tumour suppression through a distinct ferroptosis pathway. Nat Cell Biol. 2019 May;21(5):579-591. doi: 10.1038/s41556-019-0305-6. Epub 2019 Apr 8. PMID: 30962574; PMCID: PMC6624840.

37.Sarsour EH, Son JM, Kalen AL, Xiao W, Du J, Alexander MS, O'Leary BR, Cullen JJ, Goswami PC. Arachidonate 12-lipoxygenase and 12-hydroxyeicosatetraenoic acid contribute to stromal aging-induced progression of pancreatic cancer. J Biol Chem. 2020 May 15;295(20):6946-6957. doi: 10.1074/jbc.RA120.012798. Epub 2020 Apr 7. PMID: 32265301; PMCID: PMC7242692.

38.Mittler R, Darash-Yahana M, Sohn YS, Bai F, Song L, Cabantchik IZ, Jennings PA, Onuchic JN, Nechushtai R. NEET Proteins: A New Link Between Iron Metabolism, Reactive Oxygen Species, and Cancer. Antioxid Redox Signal. 2019 Mar 10;30(8):1083-1095. doi: 10.1089/ars.2018.7502. Epub 2018 Mar 29. PMID: 29463105.

39.Wang S, Wu C, Ma D, Hu Q. Identification of a ferroptosis-related gene signature (FRGS) for predicting clinical outcome in lung adenocarcinoma. PeerJ. 2021 Apr 13;9:e11233. doi: 10.7717/peerj.11233. PMID: 33954048; PMCID: PMC8051350.

40.Wu ZH, Tang Y, Yu H, Li HD. The role of ferroptosis in breast cancer patients: a comprehensive analysis. Cell Death Discovery. 2021 May 4;7(1):93. doi: 10.1038/s41420-021-00473-5. PMID: 33947836; PMCID: PMC8097021.

Tables

Table 1 The clinical statistical information of the samples.

Clinical Features	Train	Test	GSE15048
OS			
0	39	43	16
1	49	42	50
Grade			
G1	16	11	
G2	48	44	
G3	23	27	
G4	1	3	
Gender			
Male	39	40	
Female	49	45	
Age			
<=48	6	6	
>48	82	79	
M_stage			
M0	38	38	
M1	5	0	
MX	45	44	
N_stage			
N0	25	24	
N1	63	61	
T_stage			
T1	3	3	
T2	12	11	
T3	72	69	
T4	1	2	
Stage			
Stage i	10	9	

Stage ii	74	72
Stage iii	1	2
Stage iv	3	2

Due to technical limitations, Table 2 is only available as a download in the Supplemental Files section.

Figures

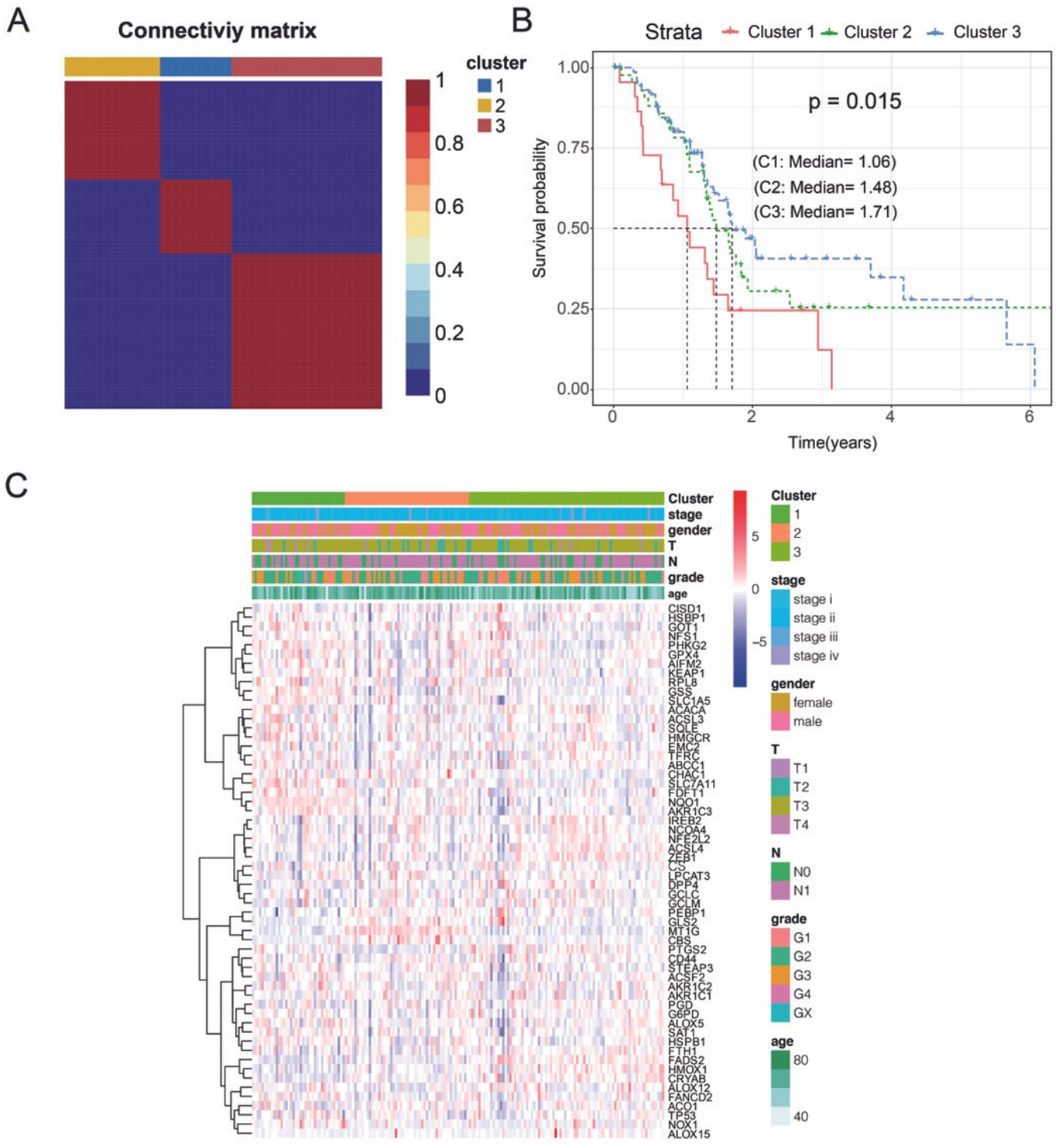

Figure 1

The expression of prognostic ferroptosis-related genes in the three categories is shown in Fig 1A. The figure shows that the expression levels of these genes are different in the 3 subtypes and that most of the genes are highly expressed in the C1 subgroup. Further analysis of the prognostic relationships between the two groups showed significant differences in C1, C2, and C3 (Fig 1B, log-rank test, $P < 0.05$). A clustering heat map of the 58 iron ferroptosis-related genes is shown in Fig 1 C.

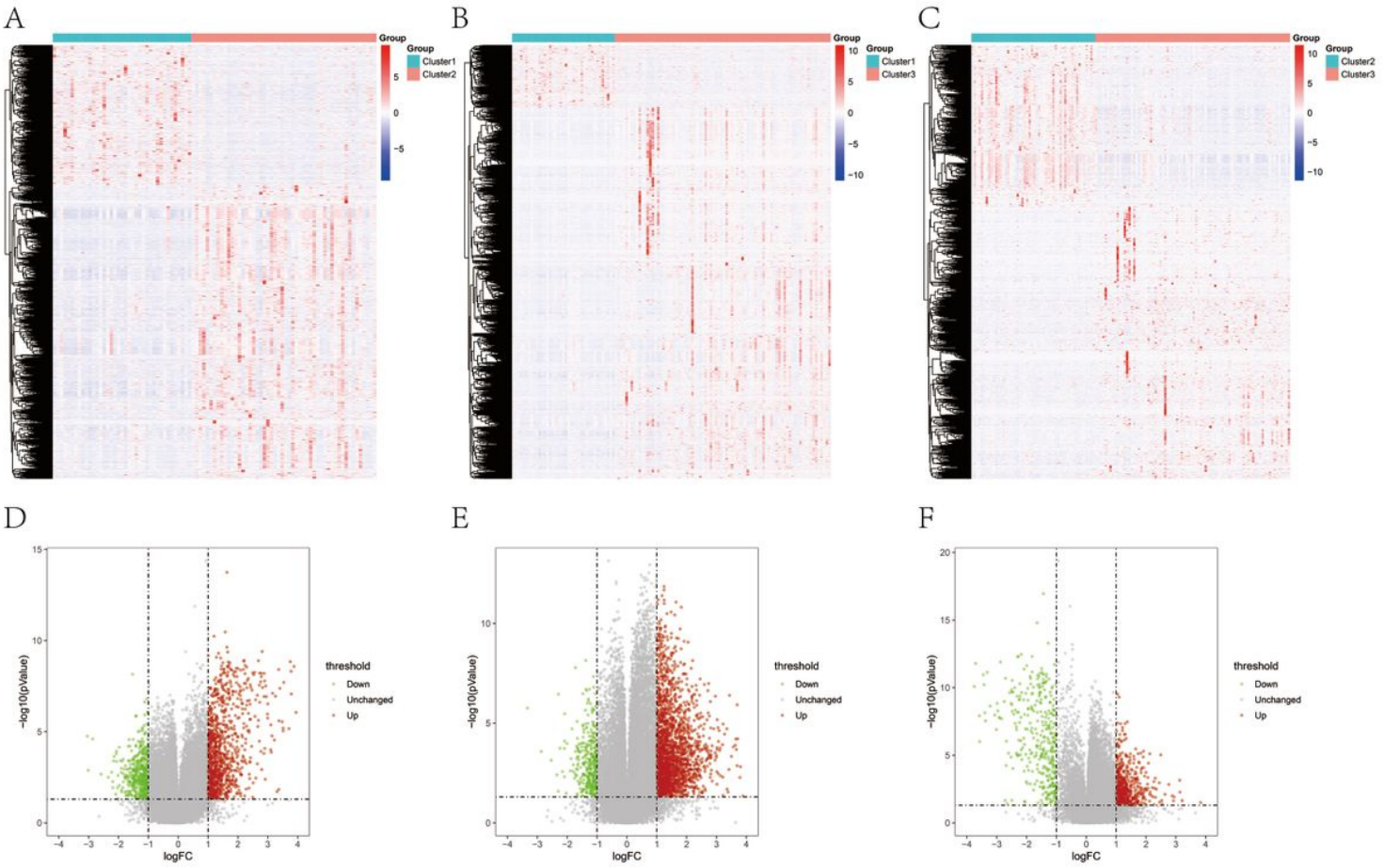

Figure 2

With the help of the limma package, 4,903 DEGs were identified between Cluster 1 and Cluster 2, among which 2,717 genes were up-regulated and 2,186 genes were down-regulated (Fig 2 A, D). There were 6,572 DEGs between Cluster 1 and Cluster 3, among which 4,963 genes were up-regulated and 1,609 genes were down-regulated (Fig 2 B, E). Between Cluster 2 and Cluster 3 there were 3,473 DEGs, among which 2,633 genes were up-regulated and 840 genes were down-regulated (Fig 2 C, F). After taking the intersection of all three clusters 230 genes were obtained

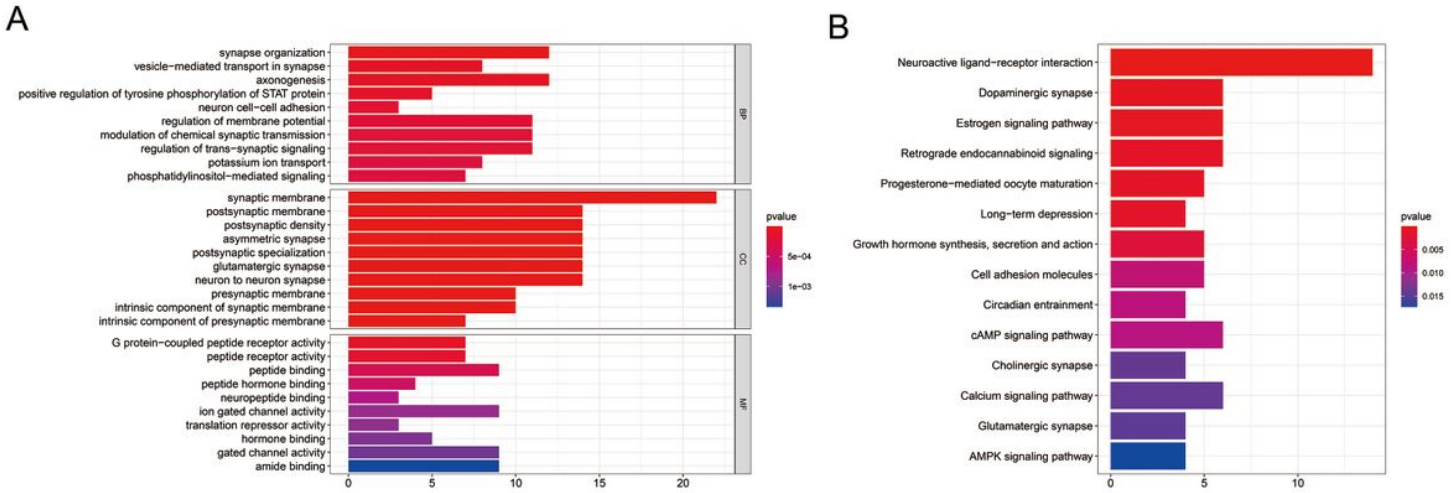

Figure 3

KEGG pathway analysis and GO functional enrichment analysis were performed on the 230 DEGs in the PAAD subtype group. A total of 179 GO-BP pathways, 47 GO-CC pathways, and 67 GO-MF pathways were annotated (Figure 3 A). 14 KEGG pathways were identified, 6 of which were significant (FDR<0.05) (Figure 3 B).

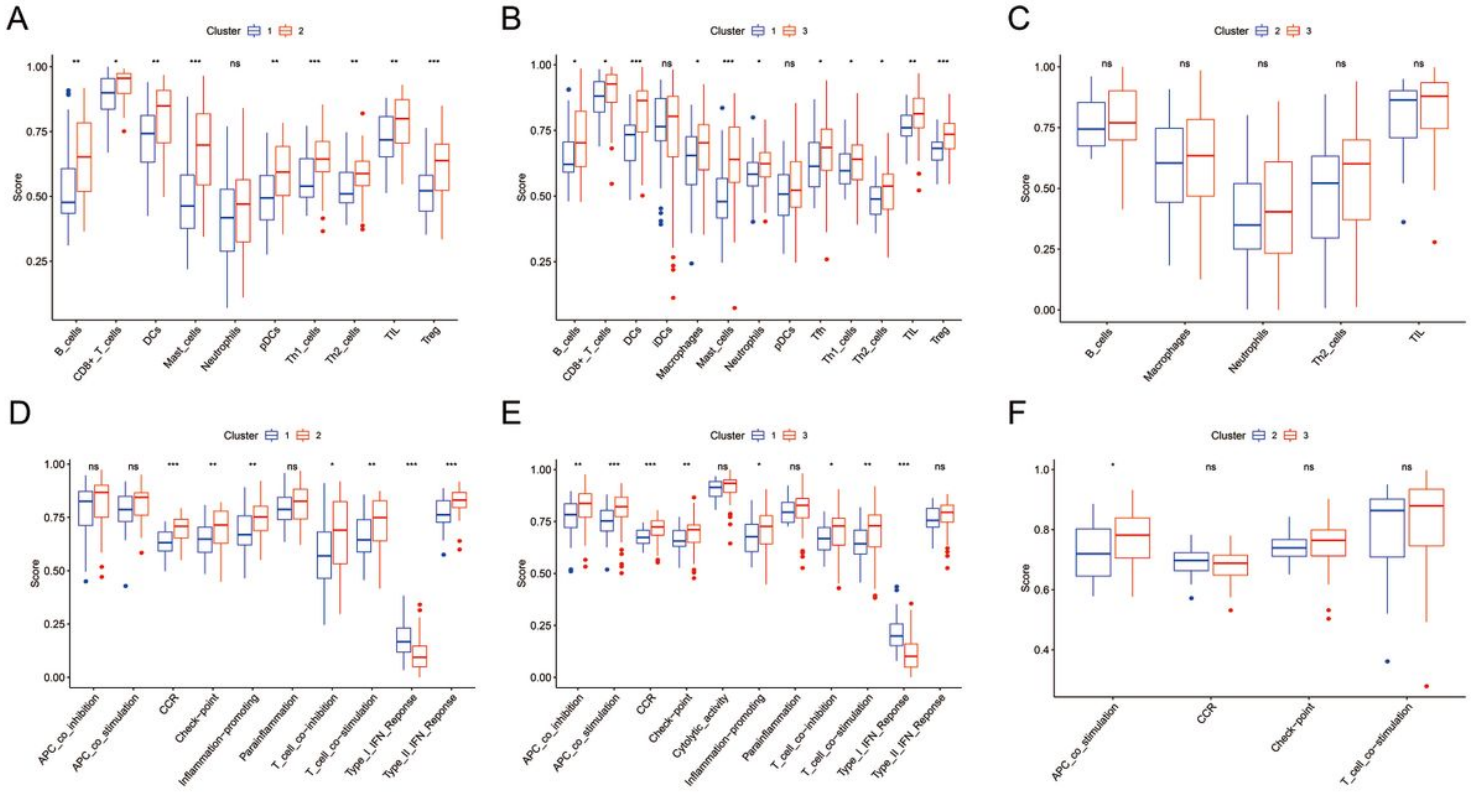

Figure 4

The immune score of the C1 subtype was lower than that of the C2 (Fig 4A) and C3 subtype (Fig 4B). The immune score of the C2 subtype was lower than that of the C3 subtype (Fig 4C). Additionally, we constructed a heat map of the immune score results for the three subtypes (Fig 4D-F).

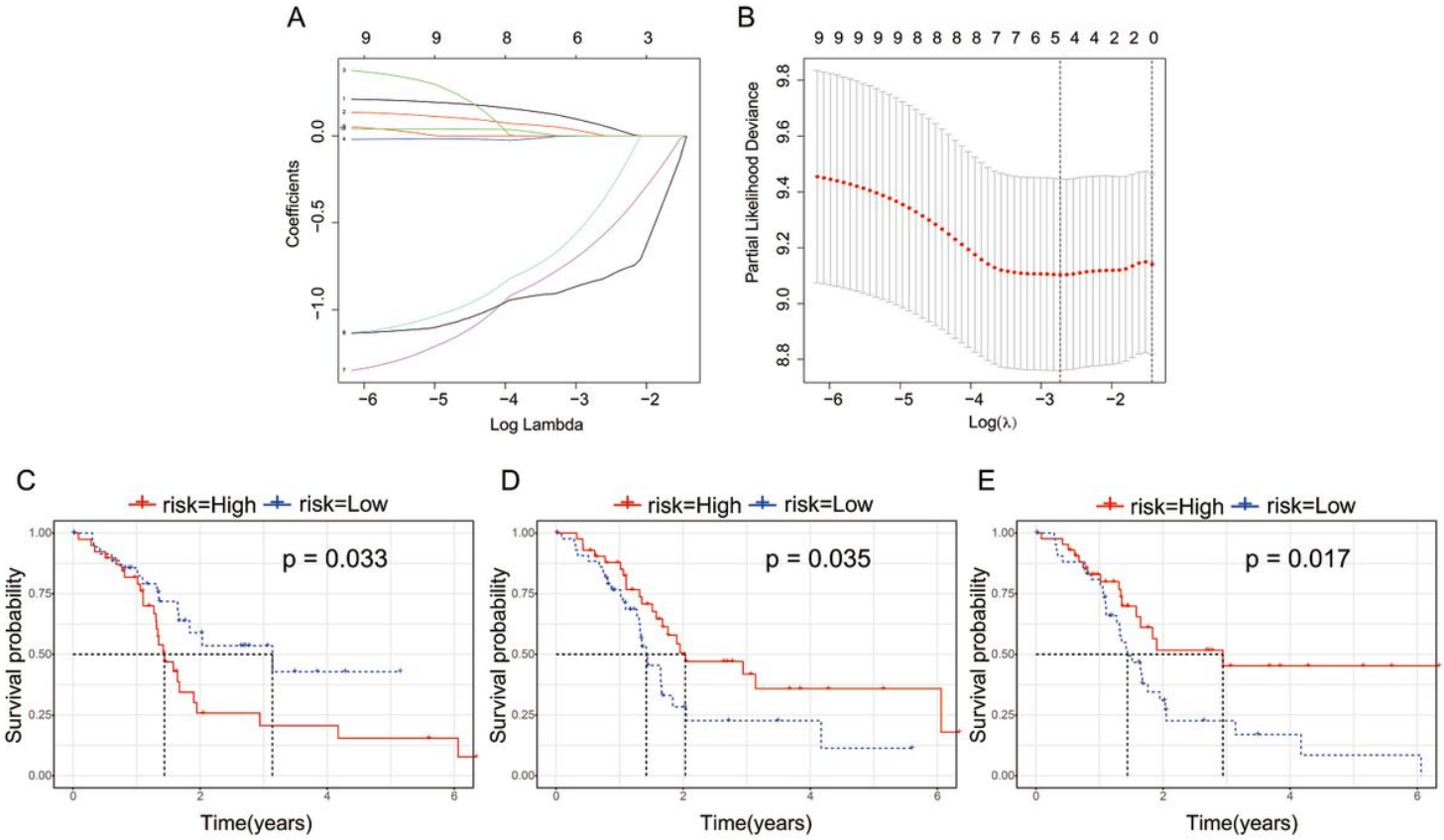

Figure 5

The changing trajectory of each independent variable is shown in Fig 5A, which indicates that with a gradual increase in lambda, the number of independent variable coefficients approaching zero gradually increases. We used 5-fold cross-validation to construct a model and analyze the confidence interval under each lambda (Fig 5B). The figure indicates that the model reached the optimal value at lambda= -3.75. Hence, we selected 5 genes at lambda= -3.75 as target genes and further selected 3 genes (ALOX5, ALOX12, and CISD1) by multivariate Cox regression analysis. Prognostic KM-curves of the three genes are shown in Fig 5C-E, and all three genes could significantly improve the performance of distinguishing between the low-risk groups (LRG) and high-risk groups (HRG) in the training sample ($P < 0.05$).

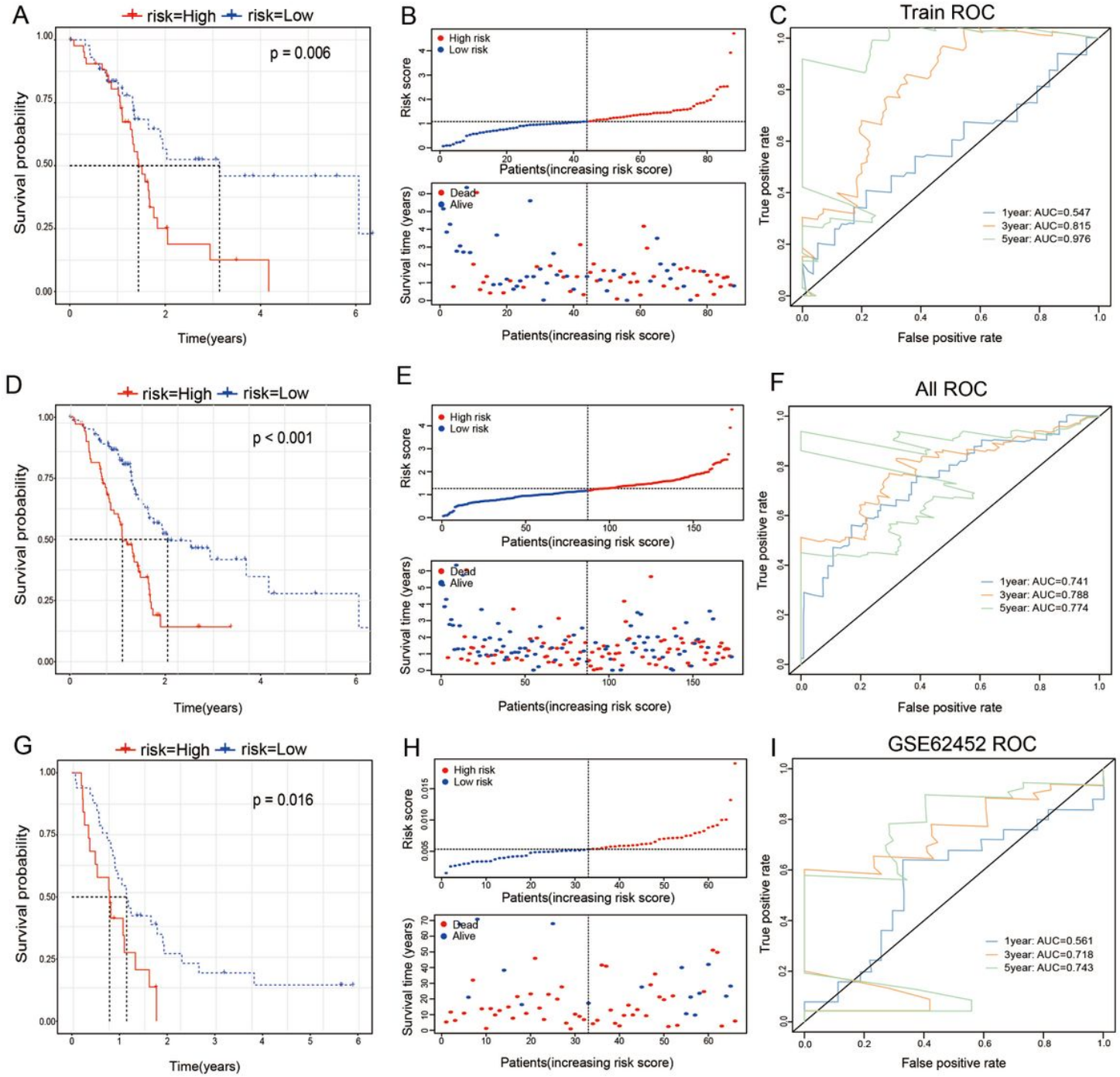

Figure 6

The risk score distribution of the training set is shown in Fig 6B. The figure indicates that the risk of death for a patient with a high-risk score was significantly higher than that of a patient with a low-risk score. This suggests that a sample with a high-risk score shows a worse prognosis. KM-curve analysis showed that there were significant differences between the high and low-risk groups (Fig 6A, P =0.006). (Fig 6C). The model had a very high AUC (AUC for 1 year=0.547, AUC for 3 years=0.815, AUC for 5 years=0.976) The risk score distribution of the entire TCGA-PAAD dataset is shown in Fig 6E, which also indicates that samples with a high-risk score had a worse prognosis. KM-curve analysis showed that there were significant differences between the high and low-risk groups (Fig 6D, P <0.001). The classification

efficiencies at 1-year, 3-years, and 5-years were 0.741, 0.788, and 0.774 (Fig 6F), respectively. Analysis of the GSE62452 showed that the risk score distribution was consistent with that of the training set and that the high-risk score samples had a worse prognosis (Fig 6H). KM-curve analysis showed that there were significant differences between the high and low-risk groups (Fig 6G, P =0.016). Analysis of the 1-year, 3-years, and 5-years prognostic prediction classification efficiencies (Fig 6I) indicated that the model had relatively high AUC at 3 years and 5 years (0.718 and 0.743, respectively).

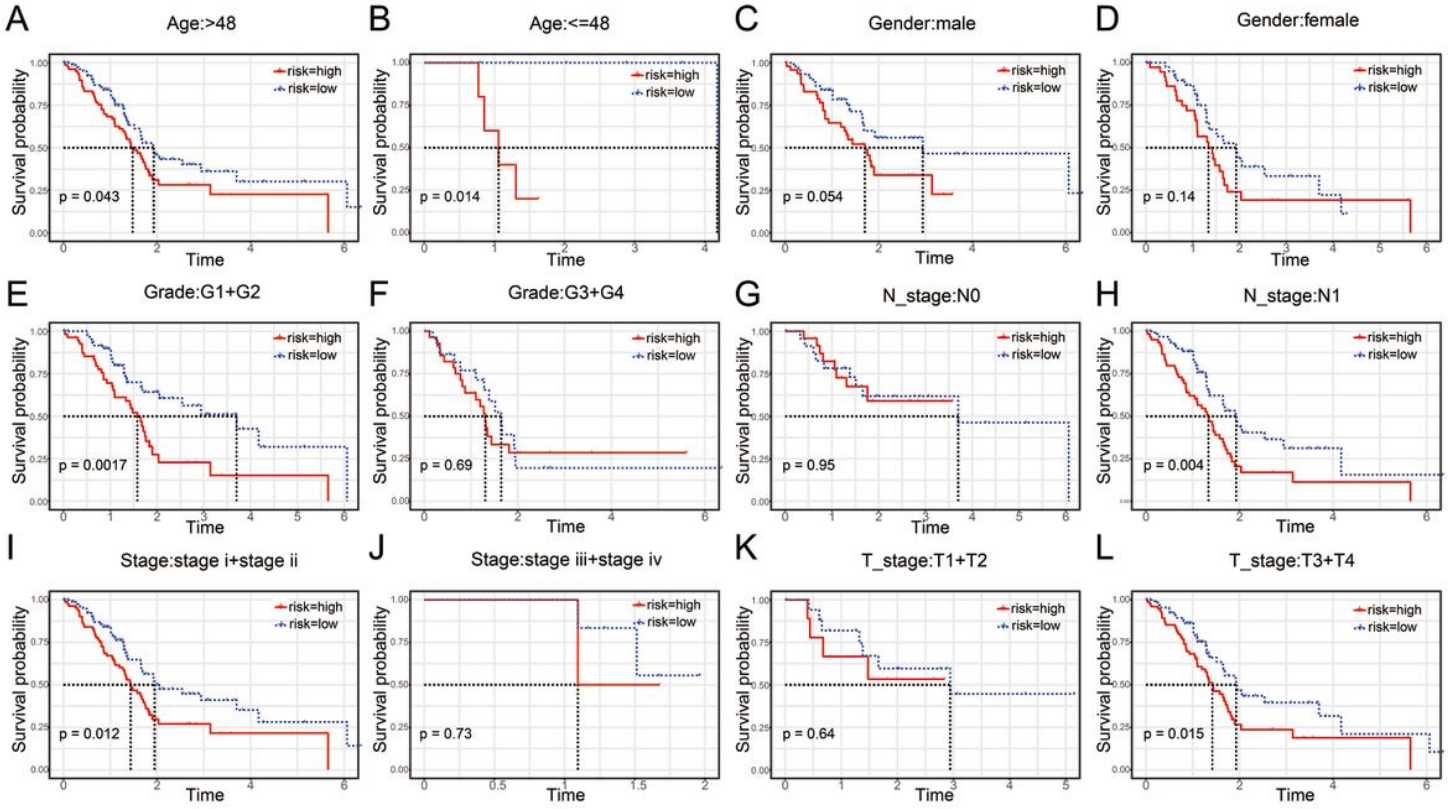

Figure 7

Based on the 3-gene signature model, samples could be divided into low- and high-risk groups according to age, sex, grade, N stage, T stage, or clinical stage (Figure 7A-L, P < 0.05).

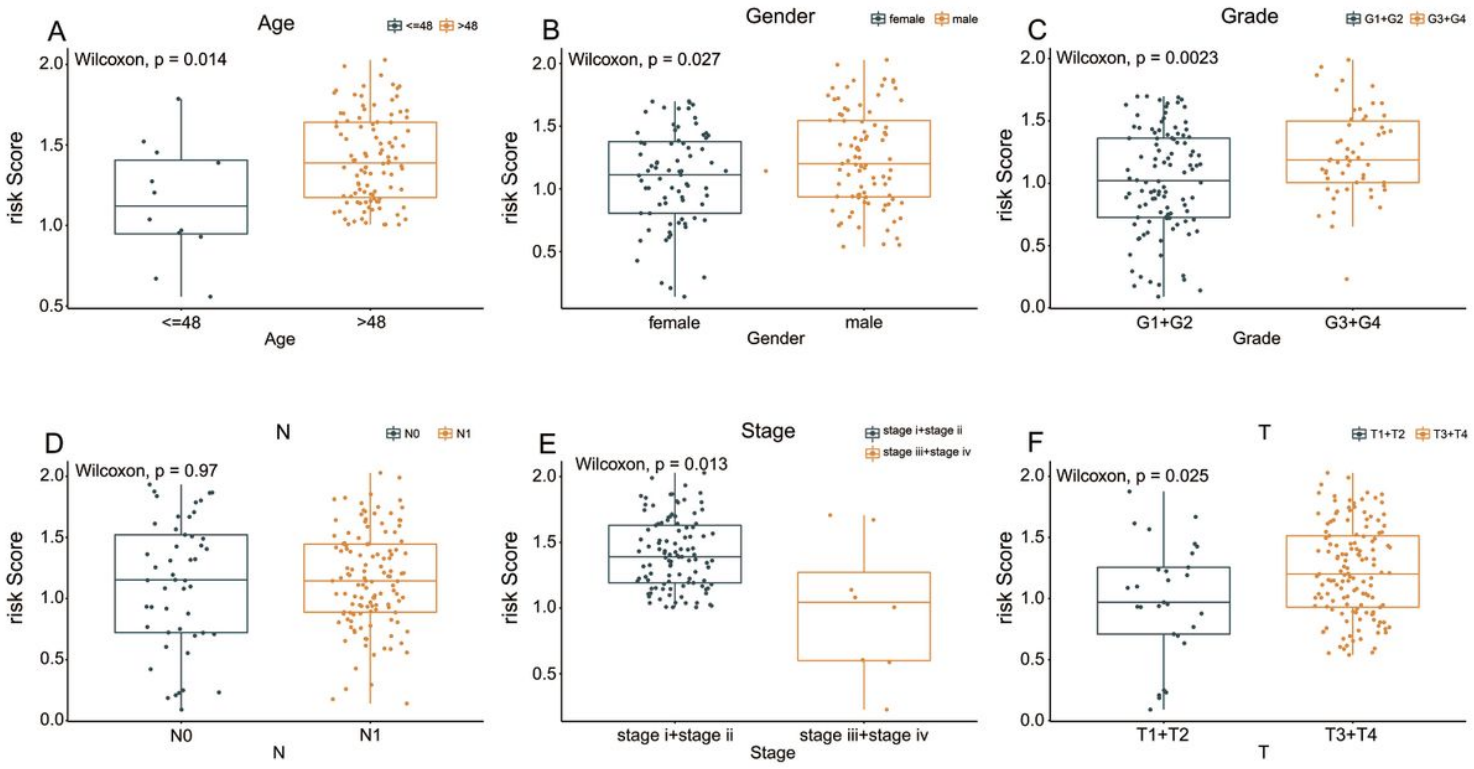

Figure 8

The risk score had a significant correlation with age, sex, grade, T stage, and clinical-stage but no significant correlation was with the N stage (Figure 8 A-F, P <0.05).

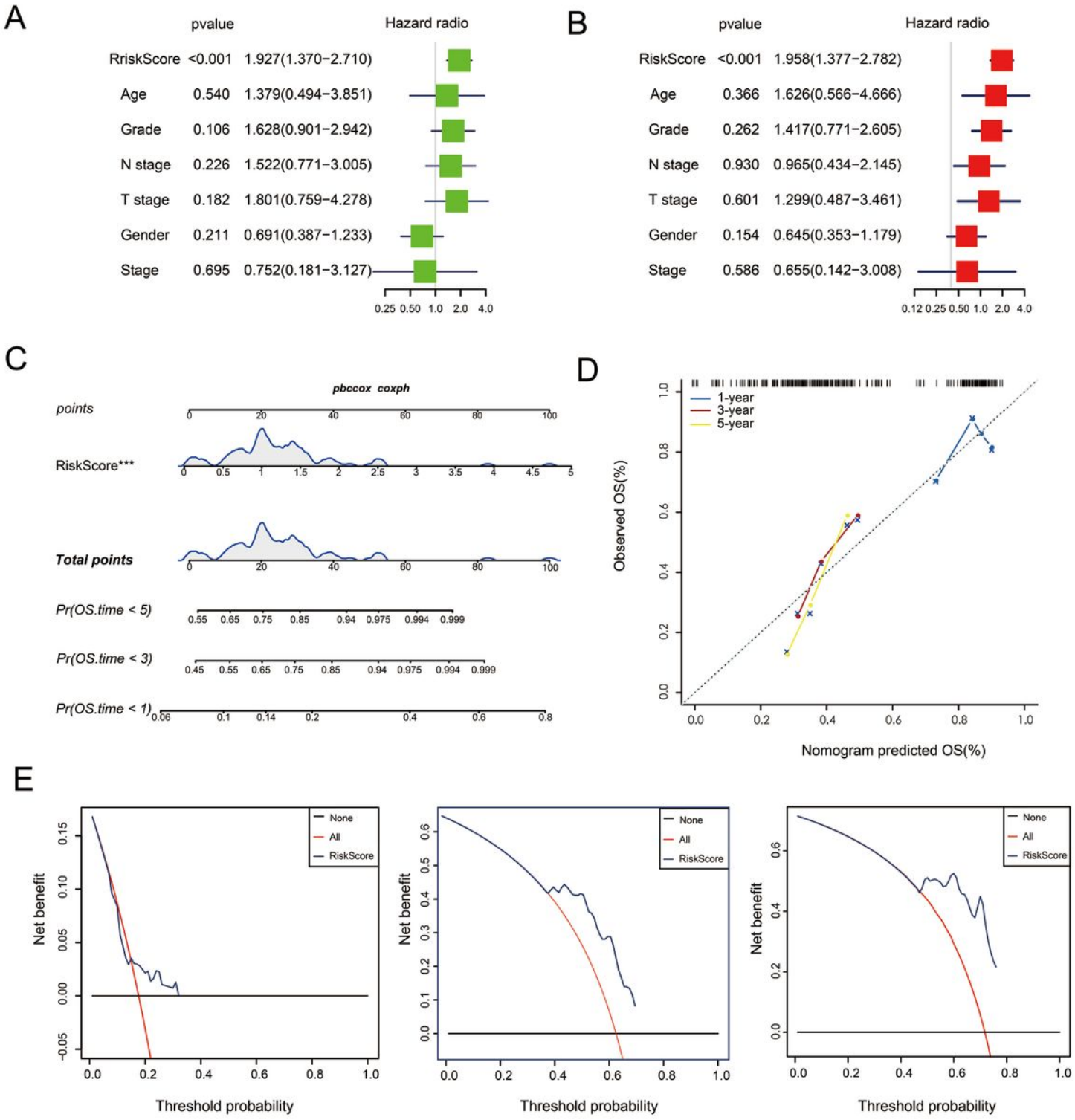

Figure 9

Both, univariate and multivariate Cox regression analyses, indicated that our model based on the 3-gene signature is an independent risk factor for prognosis in pancreatic cancer patients (Fig 9A-B). Further, the TCGA-PAAD training set was used to construct a nomogram (Fig 9C), which indicated that the risk model based on the 3 genes can accurately predict the prognosis of pancreatic cancer. In addition, we used corrected curves to analyze the prediction accuracy of the nomogram at 1, 3, and 5 years. The results

indicated that the histogram had good prediction performance (Fig 9D). Moreover, the results of decision curve analysis (DCA) at 1-year, 3-years, and 5-years (Fig 9E) also indicated that the prediction efficiency of the histogram was good.

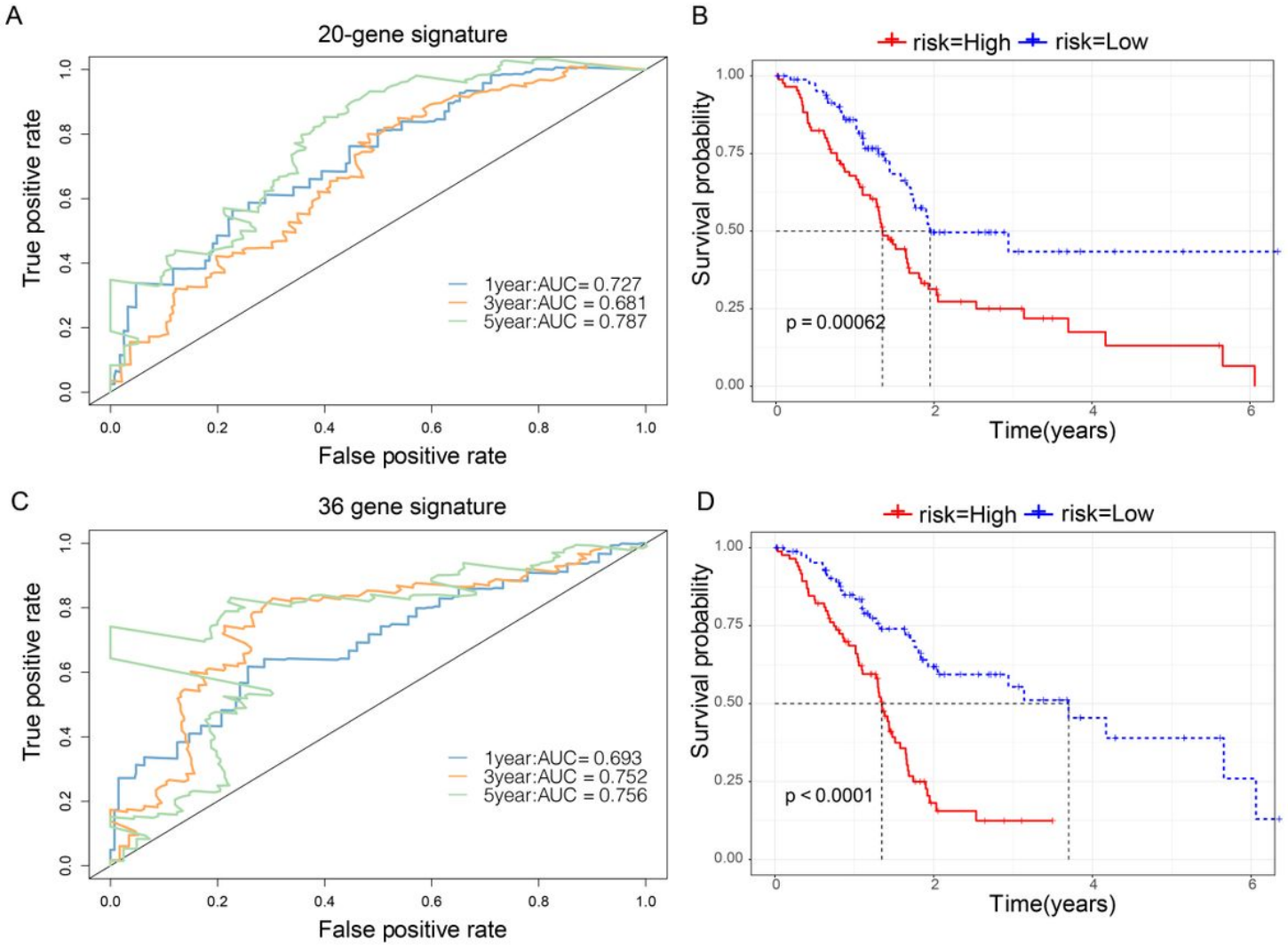

Figure 10

For the 36-gene signature model, the 1-, 3-, and 5-year AUC values were lower than our model. Moreover, the 1- and 3-year AUC values in the 20-gene signature were lower than our model. This proves that our model, with a reasonable number of genes, yields a more effective result (Figure 10).

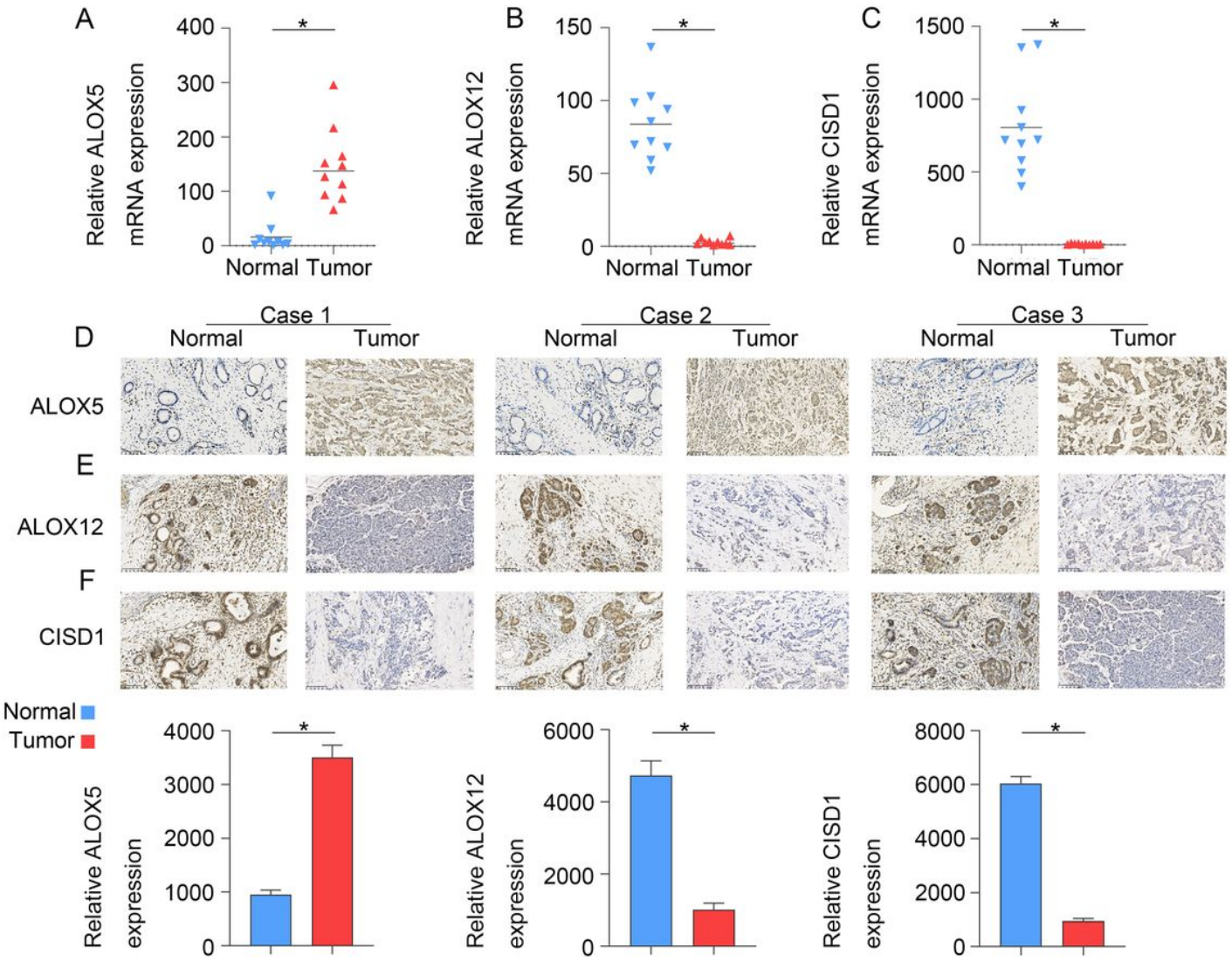

Figure 11

To verify that ALOX5 expression is upregulated and investigate whether ALOX12 and CISD1 are downregulated in pancreatic cancer tissue, 10 pancreatic cancer tissue specimens were tested. The results obtained with qPCR (Fig 11A-C) and IHC (Fig 11D-F) assays showed that ALOX5 was highly expressed regardless of whether ALOX12 and CISD1 were expressed at low levels in these pancreatic cancer tissue samples.

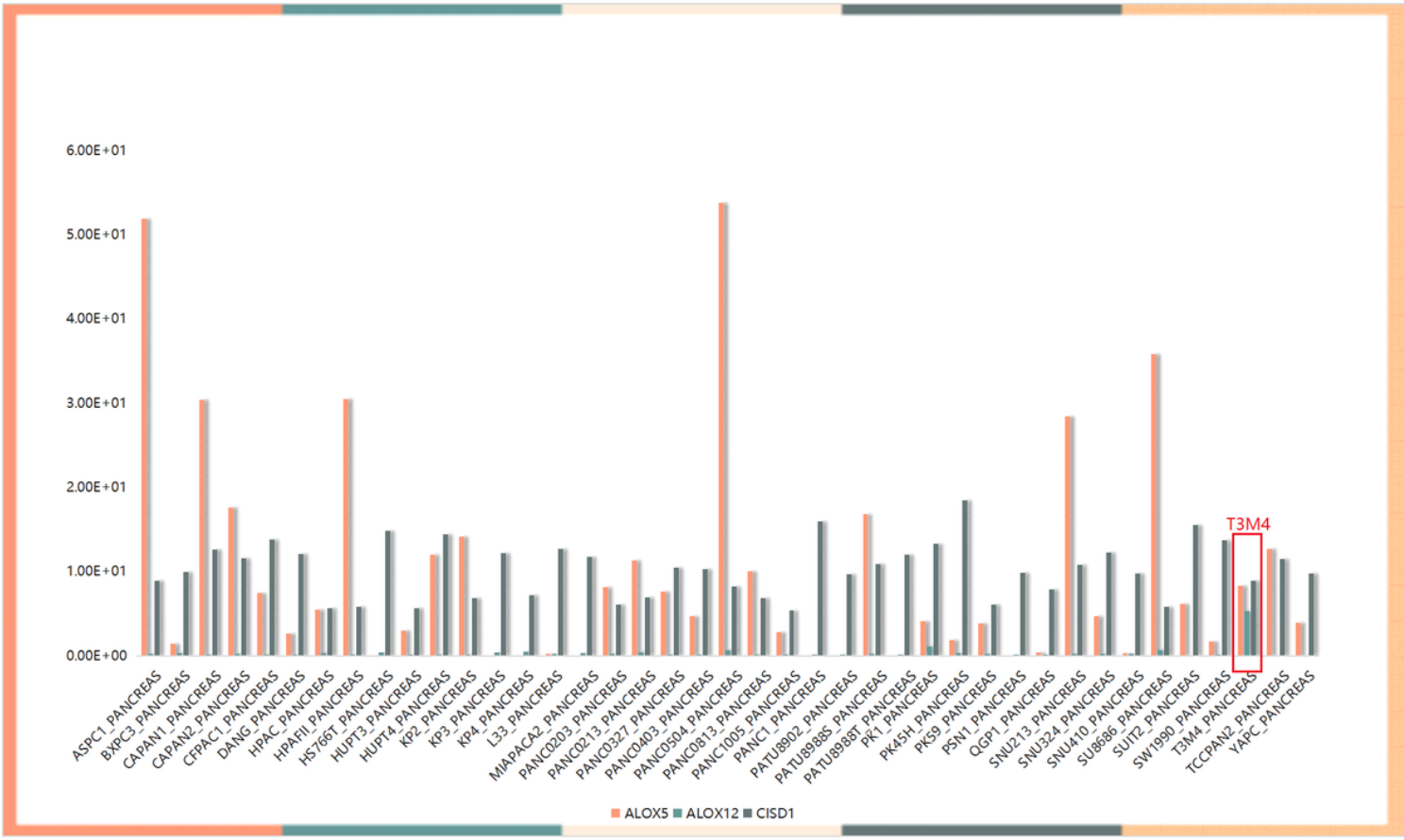

Figure 12

To clarify the functional role of signature genes in PAAD cells, we used Cancer Cell Line Encyclopedia (CCLE) database to analyze the expression of ALOX5, ALOX12 and CISD1 in pancreatic cancer cells, and found that the expression of ALOX5, ALOX12 and CISD1 was relatively highly expressed in T3M4 cells (Figure 12).

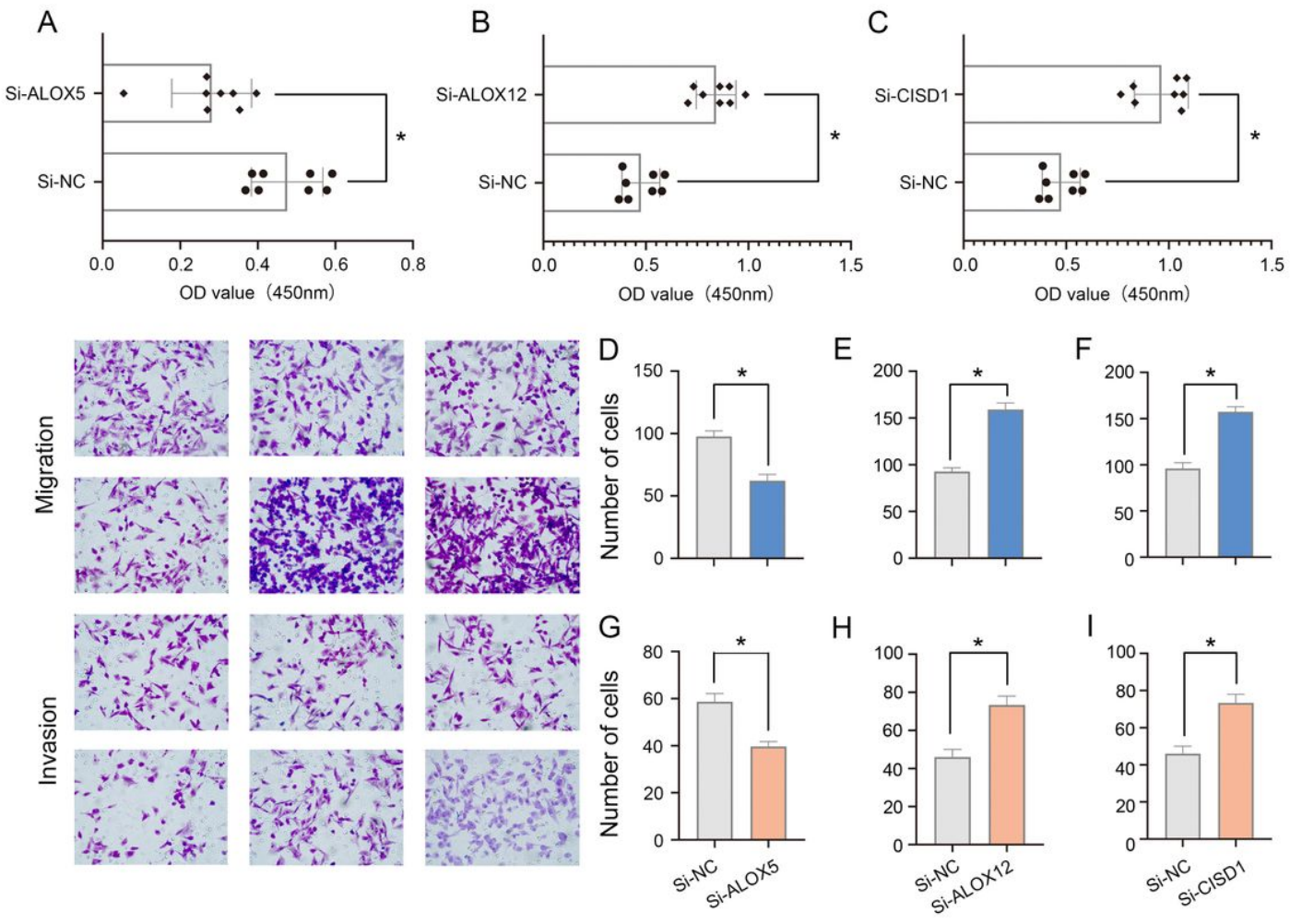

Figure 13

The results showed that reduced ALOX5 (Fig 13A, D and G) expression significantly inhibited the proliferation, invasion and migration ability of T3M4 cells ,and reduced ALOX12 (Fig 7B,E and H) and CISD1 (Fig 13C,F and I) expression significantly increased proliferation, invasion and migration ability of T3M4 cells.

Supplementary Files

This is a list of supplementary files associated with this preprint. Click to download.

- Table2.xlsx